

Full paper

Third–Generation Pleated Pneumatic Artificial Muscles for Robotic Applications: Development and Comparison with McKibben Muscle

Daniel Villegas, Michaël Van Damme*, Bram Vanderborght, Pieter Beyl and Dirk Lefeber

Vrije Universiteit Brussel, Department of Mechanical Engineering, Pleinlaan 2, 1050 Brussels, Belgium

Received 11 March 2011; accepted 2 June 2011

Abstract

This paper introduces the third generation of Pleated Pneumatic Artificial Muscles (PPAM), which has been developed to simplify the production over the first and second prototype. This type of artificial muscle was developed to overcome dry friction and material deformation, which is present in the widely used McKibben muscle. The essence of the PPAM is its pleated membrane structure which enables the muscle to work at low pressures and at large contractions. In order to validate the new PPAM generation, it has been compared with the mathematical model and the previous generation. The new production process and the use of new materials introduce improvements such as 55% reduction in the actuator's weight, a higher reliability, a 75% reduction in the production time and PPAMs can now be produced in all sizes from 4 to 50 cm. This opens the possibility to commercialize this type of muscles so others can implement it. Furthermore, a comparison with experiments between PPAM and Festo McKibben muscles is discussed. Small PPAMs present similar force ranges and larger contractions than commercially available McKibben-like muscles. The use of series arrangements of PPAMs allows for large strokes and relatively small diameters at the same time and, since PPAM 3.0 is much more light-weight than the common McKibben models made by Festo, it presents better force-to-mass and energy to mass ratios than Festo models.

© 2012 Taylor & Francis and The Robotics Society of Japan

Keywords

pneumatic artificial muscle, compliant actuation

1. Introduction

Pneumatic Artificial Muscles (PAMs) are increasingly used in a wide range of applications such as energy efficient walking robots [1,2], safe physical

*To whom correspondence should be addressed. E-mail: michael.vandamme@vub.ac.be

human–robot interaction [3,4], and rehabilitation devices [5–8]. PAMs have been considered interesting due to their variable-stiffness spring-like characteristics, physical flexibility, and very light weight compared to other kinds of actuators [9].

Several concepts of PAM have been developed over time, some examples are the Romac muscle [10], the Baldwin muscle type [11], and the most well-known type called the McKibben muscle introduced in the fifties [12]. Several forms of this type of muscle have actually been commercialized by different companies such as Bridgestone Co. [13], the Shadow Robot Company [14], Merlin Systems Corporation [15], and Festo [16]. Depending on the geometry and type of the membrane, the specific force characteristic alters.

In Fig. 1(a), the concept of the McKibben muscle is given. It contains a rubber inner tube which will expand when inflated, while a braided sleeving transfers tension. Inherent to this design is dry friction between the netting and the inner tube and deformation of the rubber tube. Typical working pressure values range from 1 to 5 bar and more. Due to a threshold of pressure which depends on the rubber characteristics, these muscles do not function properly at low pressures (e.g. pressures below 1 bar for Festo muscles).

To avoid friction and deformation of the rubber material, the Pleated Pneumatic Artificial Muscle (PPAM) was conceived and designed by Daerden [17] at the Vrije Universiteit Brussel. The membrane of this muscle is arranged into radially laid out folds that can unfurl free of radial stress when inflated. Figure 1 (b) shows the working principle of the PPAM. Its specific design presents interesting actuator characteristics but entails a complex production process, which has been considered as its major disadvantage. So far the PPAM has been used in different applications like the bipedal walking robot Lucy [18], a soft robot arm for safe HRI [3], an active ankle-foot prosthesis [19], and a step rehabilitation robot [5].

This paper presents the third generation of PPAM for which major improvements were made regarding the second generation [20]. The two former PPAM designs are briefly described to introduce the third generation, for which a simpler and more reliable manufacturing process has been developed focusing on a possible commercial production.

To evaluate the actual state of the PPAM and analyze future possibilities a comparison with the Festo fluidic muscle, a McKibben like commercially



Figure 1. (a) McKibben muscle [17] and (b) CAD drawing of the deflated and inflated state of the PPAM [20].

available muscle, is presented. For comparing actuators, in order to find the best compromise for a particular application, several factors have to be considered. The comparison presented in this paper is based in the actuators geometry and some other factors such as the tension intensity, the force-to-mass ratio, the energy to mass ratio, or the energy to volume ratio.

2. The Pleated Pneumatic Artificial Muscle

2.1. First Generation of PPAM

Daerden [17] established a mathematical model for the PPAM performance based on zero parallel stress pressurized axisymmetric membranes that was proved to be accurate with regard to the real PPAM. Due to its specific design, the PPAM can easily work from pressures as low as 20 mbar to 4 bar gauge pressure and it can reach contractions over 40%, depending on its original dimensions (theoretically 54% for an infinitely thin muscle). The muscle prototype built by Daerden [17] has a weight of about 100 g while it can generate forces up to 5 kN.

The membrane of the first generation is a fabric made of an aromatic polyamide such as Kevlar to which a thin liner is attached in order to make the membrane airtight as shown in Fig. 2(a). The high-tensile longitudinal fibres of the membrane transfer tension, while the folded structure allows the muscle to expand radially while unfurling upon inflation. The high-stiffness membrane is initially folded together and positioned into two end fittings which close the muscle and provide tubing to inflate and deflate it. The end fittings are constructed with a circular inner toothed structure to position and align each fold of the membrane, while an outer aluminum ring prevents the membrane of expanding at the end fittings. An epoxy resin fixes the membrane to the end fittings.

In Daerden's work [17], the PPAM design focused on improving the muscle performance. Extensive usage of the muscles, for example as an actuator for a



Figure 2. Photograph of three inflated states of the first-generation PPAM (a) and the second-generation PPAM (b).

bipedal walking robot, was however not immediately considered. The first prototype of PPAM needed a very complex manufacturing process that entailed a
5 insufficient lifespan. The membrane was folded while starting from a flat woven fabric, and to create a circular shape, some folds were glued together with an overlap. This overlap and the tiny length of the pleats were the main causes of the leakages that appeared during the imperfect bulging process of the pleated
10 membrane, which is shown in Fig. 2(a). Due to these utility inefficiencies a second generation of PPAM was developed.

2.2. *Second Generation of PPAM*

The second generation of PPAM was introduced while considering this actuator for a bipedal walking robot. As a solution to the leakages which caused an insufficient lifespan, the membrane composition was changed. Instead of the Kevlar fabric,
15 another more flexible material is used to create the folded membrane while the generated tension is transferred by individual high-tensile stiffness fibres that are only positioned at the bottom of each crease (see Fig. 2(b)). The pleated flexible membrane is a woven polyester cloth, which is made airtight by a polymer liner. This change makes possible to build an airtight cylindrical fabric in which the
20 folds are created afterwards. During the pleating process, separate yarns of high-tensile Kevlar fibres are positioned in every fold. This new membrane production process avoids the folded overlap, which caused several failures.

Due to the high cost of the CNC machining, the toothed inner metal tube of the end fittings of the original prototype was replaced by a straightforward aluminum basin, where the membrane was fixed by the same epoxy resin. Therefore,
25 the folds and their respective fibres were not deliberately aligned.

Lifespan tests were performed, at which muscles moves up and down a load of 130 kg by a slow varying gauge pressure between 1 and 3 bar. The lifespan of the second generation of PPAM was proved to be longer than that of the previous design. About 400,000 cycles were reached before one of the tests was
30 ended. At large number of cycles, a few Kevlar fibres were broken somewhere at the border with the end fittings, which was considered the most important failure point of the muscle. Sometimes, the epoxy of the end fittings came into the part of the fibres that was used for unfolding, making the fibres brittle at that
35 point and the fibre broke after a while.

The improved lifespan of the muscle made PPAM 2.0 useful for several applications and the Multibody Mechanics Research Group of the VUB has been using it in different robotic applications. However, the fabrication process was still too complex, causing several muscles to fail during the building, and a long
40 production time (an experimented builder required about 8 h to build one muscle), which slows the research down. Due to the impossibility of responding to demands of other researchers to build second generation's muscles for them at a reasonable price the third generation of PPAM has been developed.

2.3. Third Generation of PPAM

The third generation of PPAM, which is presented in this paper, has been developed to simplify the manufacturing process and to avoid muscle failure. The new step was partially promoted by the accessibility of Fused Deposition Modeling (FDM) rapid prototyping technology, which is used to make more complex, cheaper, and more lightweight end closures. Figure 3(a) shows the difference in design between the second and third generation. While in the second generation, a separate fibre is positioned in every pleat, a continuous high-tensile fibre is now rearranged over toothed end closures and the folded membrane. The fabric acquires the toothed shape and the fibre is positioned at the bottom of every pleat. This drastically simplifies the production process and reduces the muscle's weight even further.

Furthermore, since an external toothed part is fixed on each muscle side with epoxy, the pleated membrane is now deliberately aligned together with the fibres. Due to the toothed structure, the active part of the fibres will not be saturated with epoxy. And, therefore, the wires do not break anymore at the border with the end fittings. Because of the continuous fibre and the specifics of the production process (an inner rod is used to fix the endings during production), every fibre is of the same length and at the same tension. This results in a more symmetrical bulging (see Fig. 3(b)) of the pleated membrane and a more even distribution of the forces compared to the former generations. This together with the lower risk of broken fibres further increases the lifespan and reliability of the muscles.

The production process is drastically simplified, because the use of several small specifically designed pleating tools and the repetitive operations of making the individual fibres are avoided. The new production process is very flexible: PPAMs can now be produced in all sizes from 4 to 50 cm and the building time has been reduced to 2 h. Due to the use of 3D printing (FDM) technology for the end fittings and Dyneema fibres, this third generation PPAM is more compact and more lightweight than former generations. The muscle's weight has been

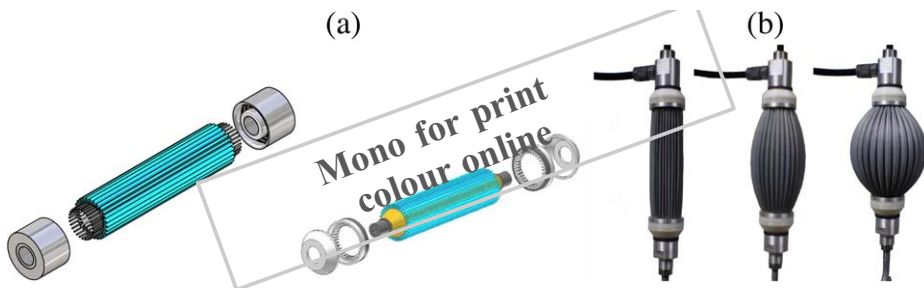


Figure 3. (a) Composition of the second and third-generation of the PPAM and (b) Photograph of three inflated states of the third-generation PPAM.

reduced by 55%, from 135 g for the second generation to 60 g for the third generation.

As was the case for the PPAM 2.0, this prototype does not incorporate neither air connector nor pressure sensor connector. An advantage of this setup is that a broken muscle can be replaced easily, keeping the connectors in the specific application frame. The end fittings of the former generations serve basically to close off the membrane ends and to keep the folds in place. In PPAM 3.0, they are also useful to pleat the membrane together with the continuous high-tensile fibre. Due to this critical role during the production process, their design has become more important. Using the FDM rapid prototyping technology, it is possible to obtain small, complex, and lightweight parts but they cannot transfer the high-tension forces generated by the muscle (forces over 5 KN have been reached). Therefore, the end fittings have to be built using parts made by 3D printing (FDM) technology together with other metal ones. The metal parts provide the pipe for the pressurized air, prevent the membrane of expanding at the end fittings during the inflation and transfer the developed tension to the connectors. And those parts made by 3D printing (FDM) technology serve to give the correct folded shape to the membrane, which determines the muscle performance as a whole.

The membrane structure is defined by its maximum length (l_0), the radius of the position of the fibres at the endings (R), and the number of pleats (n). In order to get the best actuator characteristics, the challenge is to get a PPAM with maximum slenderness ($\frac{l_0}{R}$). An increment in slenderness increases the muscle's maximum contraction, reduces the actuator's volume and diameter, and diminishes energy losses. But, on the other hand, the muscle's maximum slenderness is limited in order to be practically produced. The pleated structure has to ensure that enough material will be available for the membrane to inflate to its full extent. Therefore, the thinner or the longer the muscle, the larger the number of pleats or the higher the depth of the pleats has to be. This increases the difficulty of production and determines the maximum muscle slenderness, which is currently considered to be 10.

In most robotics applications, it is interesting to have small high-force actuators to actuate a robot with many dofs like, e.g. a hand [14,21]. In order to build small PPAMs while keeping the slenderness close to 10, it is possible to reduce the radius of the actuator by a proportional reduction of the number of pleats without reducing the pleat depth. While in the previous production process a high quantity of pleats were needed to keep the pleated shape of the membrane during the gluing and in the new manufacturing it is possible to reduce the number of pleats until a practical minimum making the production easier and faster. Therefore, it is now possible to build slender muscles with a membrane's length as small as 4 cm.

Although the radius of the muscle can be reduced, the dead volume (part of the volume that has to be pressurized when the muscle is working which does

not transfer energy to the membrane) is not avoided. Nevertheless, an advantage of the PPAM 3.0 design is that some lightweight closed parts, which might be made by 3D printing (FDM) technology, can be positioned inside the muscle membrane. This way the dead volume can be mechanically reduced while the muscle's behavior is not affected.

3. Characteristics of the PPAM 3.0

For the second generation of PPAM, the mathematical model describing the muscle characteristics, which was developed by Daerden [17], was adapted according to the new membrane design [20]. While the original model assumed a continuous axisymmetrical circular membrane, the new model assumes that the tension is only transferred by the finite number of high-tensile strength longitudinal fibres neglecting any influence of the pleated airtight polyester membrane. Due to the differences in the initial assumptions, the new expressions of the generated tension and fibre stress depend on the number of pleats. However, the resulting analytical solution is almost identical for large numbers of discrete fibres. If the number of used fibres is greater than 15, the difference between the two models is less than 3% [20]. Since the design of the membrane has not changed, the same mathematical model is assumed for PPAM 3.0 and validated in this section.

As derived in [20] the generated force F equals:

$$F = pl_0^2 \frac{n}{2\pi} \sin\left(\frac{2\pi}{n}\right) f\left(\epsilon, \frac{l_0}{R}\right) \quad (1)$$

with $f\left(\epsilon, \frac{l_0}{R}\right)$ the dimensionless force function as defined by Daerden [17]. The contraction is defined as $\epsilon = \frac{l_0 - l}{l_0}$, l_0 is the maximum length of the muscle's membrane and R represents the minimum muscle, radius. $\frac{l_0}{R}$ is called the slenderness, p is the relative pressure inside the muscle and n is the number of fibres used. This function f depends only on contraction and geometry as far as the elasticity of the fibres is neglected. The thicker the muscle, the less it contracts and the higher the forces it generates in short contractions. Contraction can reach up to 54% in a theoretical case with $\frac{l_0}{R} = \infty$, which is bounded in practice because of minimum space needed to fold the membrane.

Static load tests on real muscles were carried out to validate the proposed mathematical model of Equation (1). Four standard muscles were tested on different contraction trajectories between ≈ 150 N and ≈ 3 KN with a test bench at isobaric conditions, while applying three different gauge pressures: 1–3 bar. The tested muscles are made with 32 pleats, have a maximum membrane length $l_0 = 110$ mm and unpressurized radius of 15.6 mm at the top of the polyester fabric pleats and $R = 11.5$ mm for the position of the Dyneema fibres. One side of

the muscle is fixed to the load cell while the other side is attached to a movable frame. The tests are performed by controlling the displacement of an INSTRON 4505 tensile test bench. During each test, frame position, muscle force, and applied gauge pressure are recorded. The forces are recorded with a load cell with a maximum range of 10 kN and the pressure inside the muscle is regulated by a pressure servovalve (Kolvenbach KPS 3/6). The pressure inside the muscle is measured by a gauge pressure sensor (SensorTechnics BSDX5000G2R).

As can be seen in Fig. 4(a), the repeatability between muscles is successful. But, as in the tests carried out on the second generation prototypes [20], an unmodeled hysteresis effect is noticed (see Section 4.2). It is seen that the different curves show a more or less comparable hysteresis width.

The approximation of the real force with the mathematical model is suitable enough for dimensioning purposes but it is not used as a model in controllers and simulations. The dimensionless function $f(\epsilon, \frac{l_0}{R})$ is not available in closed (or analytical) form and, in order to evaluate it for given ϵ , $\frac{l_0}{R}$, and n , a system of equations involving elliptic integrals has to be solved numerically (see [17,20]). Due to it, the theoretical dimensionless force function is replaced with a 4th order polynomial fit $f(\epsilon)$ on the measured data. With the incorporation of pressure p and the square of the initial muscle length l_0^2 the dimensionless force function of muscles with a specific slenderness can be polynomially estimated. And the output force of PPAMs can be expressed as:

$$F = pl_0^2 f(\epsilon) = pl_0^2 (f_4 \epsilon^3 + f_3 \epsilon^2 + f_2 \epsilon + f_1 + f_0 \epsilon^{-1}) \quad (2)$$

with f_0 to f_4 the five coefficients resulting from a fourth order polynomial approximation.

Due to the pressure regulating valve, the actual pressure during each test run is not exactly the same. To overcome this, it is better to compare the test results by dividing the measured forces by the measured pressures. Figure 4(b) shows

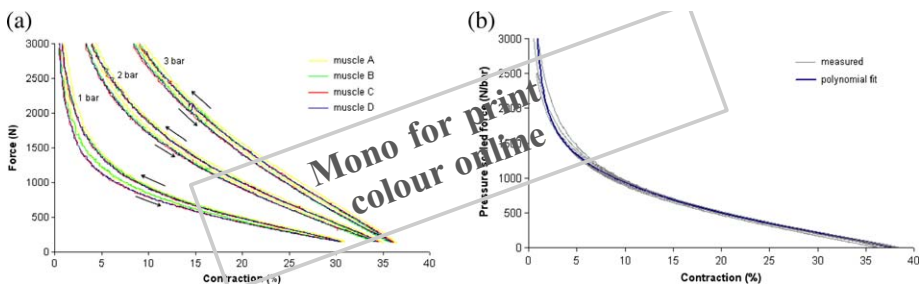


Figure 4. (a) Measured forces as a function of contraction for four muscles with 32 pleats at pressure levels 1–3 bar and (b) Pressure scaled measured forces for PPAM 3.0 prototypes as a function of contraction compared with polynomial-fitted estimation.

all the pressure scaled force measurements in comparison with the estimated pressure scaled force function.

As was done by Verrelst et al. [20] for the second generation of PPAM, the polynomial function fit is compared with theoretical graphs to evaluate the practical slenderness of the prototypes. In both generations, the prototypes are built to have a physical membrane length $l_0 = 110$ mm and an unpressurized radius $R = 11.5$ mm for the position of the Kevlar fibres, which entail a theoretical slenderness value of 9.6. Using these dimensions in Equation (1) results in the theoretical force graphs depicted in Fig. 5. Since the muscle length is easily measured, the model validation is done regarding the radius value.

While Verrelst et al. concluded that the best model to represent the actual generated force of the PPAM 2.0 was to use as R the radius at the top of the polyester fabric pleats: 16 mm, it is observed that the measurements on the third-generation prototypes can be represented by the theoretical model with $R = 11.5$ mm. Therefore, the prototypes of the third generation present force-contraction characteristics of a more slender muscle than the previous generation. This improvement is due to the deliberated positioning and fixing of the fibers in the new production process.

As the theoretical model can be used for dimensioning purposes, it is also useful for comparing different prototype designs. Figure 5 shows that the same kind of differences between the polynomial fit on measured data and the theoretical dimensionless force function are identified in both generations. At high forces, the theoretical model presents shorter contractions than the polynomial fitted estimations and, at high contractions, the prototypes develop smaller forces than those theoretically expected. These differences are due to the hysteresis, the materials' elasticity, and the radial stress in the polyester membrane, which were neglected in the model.

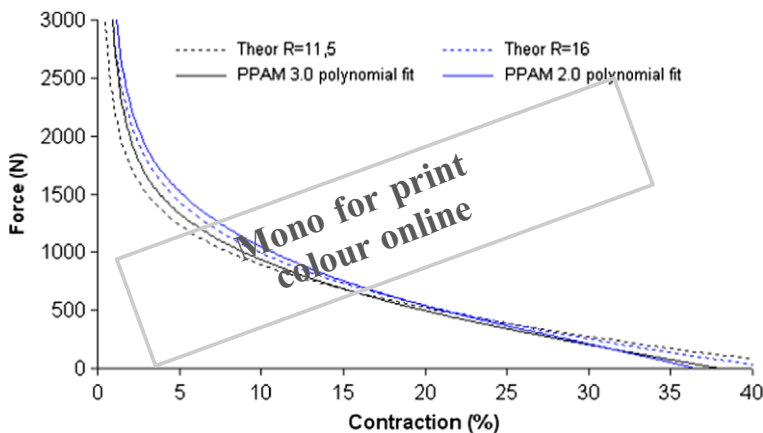


Figure 5. Polynomial-fitted estimations of PPAM 2.0 and PPAM 3.0 as a function of contraction compared with theoretical model.

Table 1.

Coefficients of the polynomial force function approximation of the PPAM 3.0

f_4	f_3	f_2	f_1	f_0
-0.01239	1.20689	-63.3143	1299.36	1613.48

The coefficients of the fitting process for the force function of the third generation PPAM, following the structure of Equation (2), are given in Table 1. The values are valid when the generated force F is expressed in N, the initial muscle length l_0 in m, the pressure expressed in bar, and the contraction ϵ expressed in %.

The data in Table 1, together with Equation (2), can only be used to generate an approximation of the force characteristics for scaled muscles with a specific slenderness ($l_0/R = 110/11.5 = 9.6$).

4. Comparison Between McKibben and PPAM Muscle

In the previous sections, we have shown the evolution of the PPAM towards a powerful and reliable actuator. To evaluate the current state and possibilities of PPAMs, the new design of PPAM is compared with the most widespread PAM: the McKibben muscle. The general behavior of PAMs with regard to shape, contraction, and tension when inflated will depend on its membrane design. Due to the different working principles and membrane structures, it is impossible to do a complete comparison taking into account all the parameters of these two PAM actuator types. While the force-contraction characteristics of a PPAM are characterized by the slenderness ($\frac{l_0}{R}$) and the length (l_0) of the muscle, see Equation (1), those of a McKibben muscle are not dependent on the muscle's length and are only characterized by its diameter at a maximum braid angle of 90° , D_0 [9]:

$$F = \frac{pD_0^2\pi}{4}(3\cos^2\theta - 1) \quad (3)$$

This paper presents a comparison between a McKibben-like commercially available muscle, the Festo fluidic muscle, and PPAM to evaluate their strong points and drawbacks depending on the application. Different configurations of scaled PPAM 3.0 with slenderness value of 9.6 are compared with Festo models with diameter values of 10, 20, and 40 mm on the basis of external characteristics and ratios, which are interesting for the user.

We compared the third generation PPAM with the Festo fluidic muscles because they are the most widely used commercially available McKibben muscles. It should be noted, however, that McKibben muscles available from other

brands (e.g. Shadow and Merlin) may have different characteristics than the considered Festo muscles.

4.1. Force-Contraction Characteristics

In order to compare the force-contraction characteristics of these two types of pneumatic muscles, Fig. 6(a) gives the results of static load tests which were carried out with commercially available Festo muscles (DMSP-10-100N, DMSP-20-150N, and DMSP-40-200N) and PPAMs prototypes ($l_0/R = 9.56$, $l_0 = 110$ mm) on the same pressure levels: 1–4 bar. Although Festo muscles are able to work at higher pressures, 8 bar for DMSP-10-XXX and 6 bar for DMSP-20-XXX and DMSP-40-XXX, the upper pressure limit of 4 bar has been chosen to compare both muscle types at reliable pressure levels. Force and contraction ranges reported by Festo [16] were respected during the testing. And, since the PPAM is theoretically able to develop extremely high forces, the maximum tension F_{\max} was practically limited to 5 kN according to the cross-section area and mechanical properties of the prototypes' metal endings.

While the practical maximum contraction of Festo muscles is highly dependent on the working pressure, with a maximum limit of 25%, that of PPAM only differs by 2% from 1 to 4 bar reaching practical contractions over 38%. Due to the pleated membrane structure, the maximum contraction of a PPAM depends

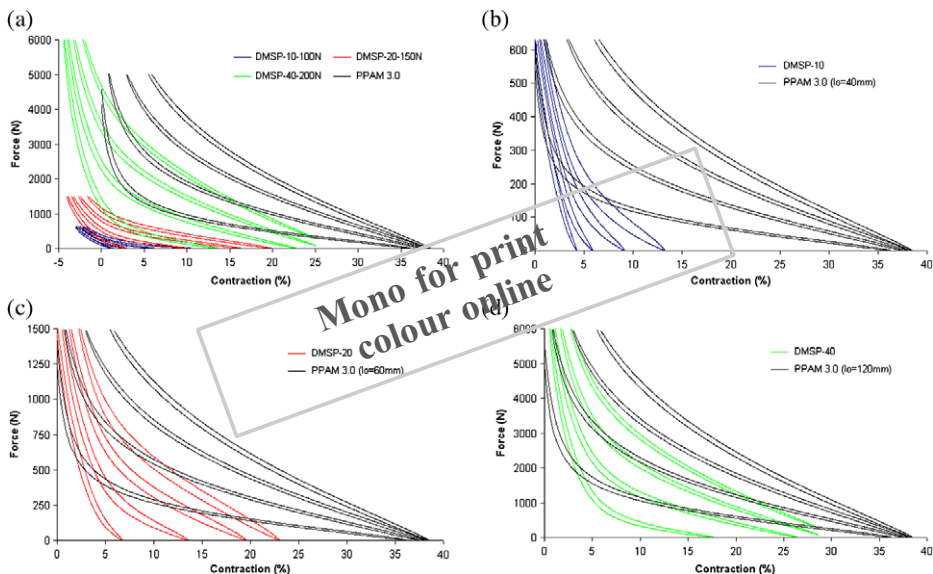


Figure 6. (a) Measured forces as a function of contraction for PPAM 3.0 and Festo products: DMSP-10-100N, DMSP-20-150N, and DMSP-40-200N at pressure levels 1–4 bar, (b) measured forces for Festo DMSP-10 and scaled measured forces for PPAM 3.0 of $l_0=40$ mm as a function of contraction at pressure levels 1–4 bar, (c) same as, (b) but for Festo DMSP-20 and $l_0 = 60$ mm, and (d) same as (b) but for Festo DMSP-40 and $l_0 = 120$ mm.

5 on its slenderness and PPAMs of slenderness higher than 3 will reach higher contractions than Festo muscles. Another important difference is that, due to their elastic components, Festo muscles are able to work slightly elongated when the actuator is fixed to the structure in a pretensioned state, which is not possible for PPAM due to the inelasticity of the fibres.

10 In order to compare both muscle's types at different strokes and force ranges, the measured data can be extrapolated to different scales and configurations of muscles. In the case of the PPAM, according to Equation (1), the PPAM's force measurements can be scaled by l_0^2 for muscles with a specific slenderness value of 9.6. And, as the maximum tension F_{\max} is proportional to the cross section-area of the endings (πR^2), which is also proportional to l_0^2 for a specific slenderness, it is possible to dimension PPAMs which have similar force ranges than Festo models. For instance, PPAMs of lengths of 40, 60, and 120 mm and slenderness values of 9.6 will have similar force ranges than the DMSP-10-XXX, DMSP-20-XXX, and DMSP-40-XXX, respectively. Furthermore, in the follow-
15 20 ing analysis the contraction of Festo muscles is referred to their maximum length, which is more representative for a real setup because it is the length which will determine the distance between its connectors for a complete use of the muscle's properties.

25 Figure 6(b)–(d) shows the force-contraction characteristics of Festo muscles and specifically scaled PPAMs. Comparing actuators with the same force ranges it is seen that PPAMs exert higher forces and reach higher contractions than Festo muscles. However, while the measured data of each Festo model can be used for any stroke range (the force-contraction characteristics of McKibben muscles do not depend on the muscle's length), those of PPAMs are only valid for a specific muscle's length.

30 To compare both muscle's types at higher strokes, it is possible to analyze a series arrangement of PPAMs (which has been used in a soft robot arm for safe physical HRI [3] and a step rehabilitation robot [5]). As can be seen in Fig. 7, these actuators were built using rings to divide a long membrane into a few modules with the desired geometry. A series of M identical PPAMs exerts the
35

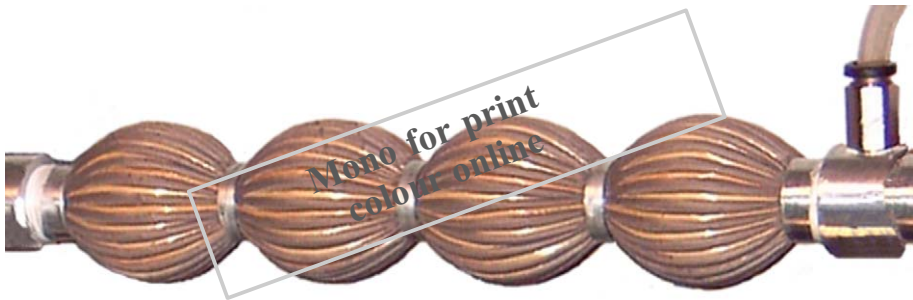


Figure 7. Photograph of a series arrangement of four modules of the second generation PPAM.

same force as a single muscle, but the total shortening is M times larger. This allows for large contractions and relatively small diameters (when inflated) at the same time.

To characterize the force-contraction characteristics of any series arrangement of PPAMs the fact that the rings positioned between the modules do not contract has to be taken into account. The contraction of a series configuration of PPAMs is slightly reduced but still reaches contractions over 34% even in a series of a high number of short modules (for instance series of 20 modules of the shortest muscle type ($l_0 = 40$ mm)). Figure 8 presents a comparison between actuators of the same initial length at 3 bar, for which both muscle types reach their maximum contractions. Due to the difference in maximum contraction, PPAM actuators will reach higher strokes than Festo muscles of any length or, a shorter PPAM will reach the same stroke than a Festo muscle with the same force range. Besides, PPAMs can develop higher forces at medium and large contractions than Festo muscles.

4.2. Hysteresis

The hysteresis represents an energy loss and a problem to estimate the behavior of pneumatic muscle-based systems. Theoretically, the measured pressure could be used to estimate the force exerted by the actuator but the hysteresis, which is not included in the theoretical models, can make the estimates too inaccurate to be useful in feedback control strategies. While the hysteresis is inherent in McKibben muscle because of its elastic components, the high-tensile materials used in the PPAM and its pleated structure might reduce this drawback. However, in reality, hysteresis is also present in all PPAM generations. Both muscle types present a similar hysteresis which is considered as a maximum error of 5% on the estimated force function.

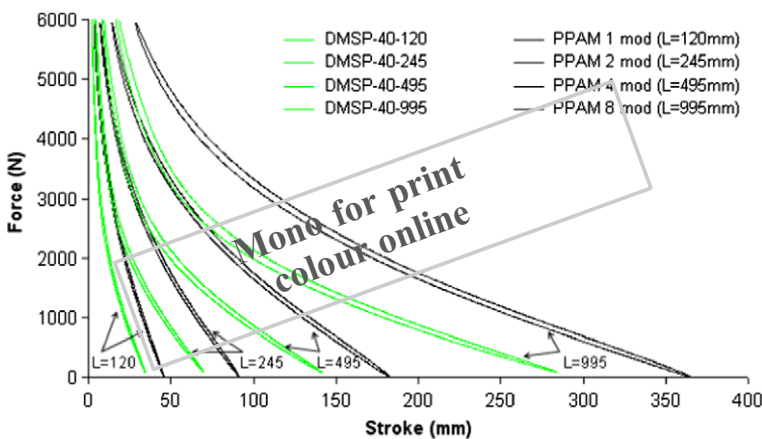


Figure 8. ForceStroke comparison between PPAM series arrangements and Festo actuators of the same initial length at 3 bar.

Different studies have analyzed hysteresis in both artificial muscles types in order to determine whether it is caused by Coulomb or viscous friction and to introduce it in the theoretical models. In spite of the different working principles, the velocity independence, which was shown by testing the muscles at different inflation frequencies, indicates that hysteresis is dominated by Coulomb friction in both muscle types. While the main causes for hysteresis in the McKibben muscle are friction between the braided mesh shell and the internal bladder and friction between braid strands [9,22], Van Damme et al. [23] report that hysteresis in PPAMs may be caused by friction between the fibres and the membrane and the unfolding of the pleats. They also developed a Preisach-based model to represent PPAM hysteresis which is considered accurate enough for contractions between 7 and 20% (which is the range mostly used in applications).

4.3. Volume and Diameter

As was mentioned above, the shape of a PAM when inflated will depend on its membrane structures and working principles. While the shell structure of a McKibben muscle will keep the muscle with a cylindrical shape during the inflation, the almost complete lack of material deformation and almost zero parallel stress present in the PPAM define its contracted shape as a spheroid. Therefore, while the diameter of a McKibben muscle does not depend on its maximum length and its volume is proportional to it, a PPAM blows up to a diameter of the same order of magnitude as its maximum length l_0 as it contracts. The equatorial diameter D and volume V of a PPAM are defined as:

$$D = l_0 d_0 \left(\epsilon, \frac{l_0}{R} \right) \quad (4)$$

$$V = l_0^3 v_0 \left(\epsilon, \frac{l_0}{R} \right) \quad (5)$$

with $d_0 \left(\epsilon, \frac{l_0}{R} \right)$ and $v_0 \left(\epsilon, \frac{l_0}{R} \right)$ dimensionless functions established by Daerden [17].

Some advantages of the smaller bulging of McKibben muscles are that many muscles can be used close to each other, as is the case in e.g. the shadow hand [14], or can be positioned close to the moving structure or human body parts, as is the case in rehabilitation. In order to be suitable for these applications in which the maximum diameter is limited, PPAMs are used in a series configuration. The rings (see Section 4.1) limit the bulging of the muscle reaching diameter values of the same order of magnitude as the module's length l_0 . However, as can be seen in Fig. 9(a), the maximum diameter of PPAMs modules are slightly larger than those of Festo products of the same force ranges.

Due to the different muscles' geometries, long single PPAMs are more voluminous than McKibben muscles of the same length but they are also able to

develop much higher forces than Festo models. In order to analyze actuators with the same force ranges Festo models are compared with PPAMs of 40, 60 and 120 mm length. Although the length of a McKibben-like muscle does not affect to its force range, it is proportional to its volume and therefore, the volume comparison has to be done according to the muscle's length. Figure 9(b) shows that the volume of a PPAM is similar to that of a McKibben muscle of the same length and same force range.

The use of a series arrangement enables PPAM's actuators to reach high strokes and reduces their volume. The total actuator's volume includes the sum of that of the M modules and the internal volume of the part of the membrane which is surrounded by the rings:

$$V = Ml_0^3 v_0 \left(\epsilon, \frac{l_0}{R} \right) + (M - 1)\pi R^2 l_r \quad (6)$$

with l_r the length of one ring. The total actuator's volume is almost proportional to the maximum length of the actuator ($Ml_0 + (M - 1)l_r$), as is the case of a McKibben muscle, and the results can be extrapolated to different strokes.

4.4. Tension Intensity

The tension intensity is defined as the ratio of the actuator's maximum output force and the actuator's maximum cross-section area [9]. It is an indicator of radial compactness, which is needed to use many muscles close to each other. Since the maximum forces are exerted at small contractions, the further a muscle contracts, the more reduced this ratio is.

Since the maximum diameter and maximum output force of McKibben muscles do not depend on the maximum muscle length, the tension intensity curve (tension intensity as a function of contraction) is the same for each Festo model. For instance, although a DMSP-10-500 is five times longer than a

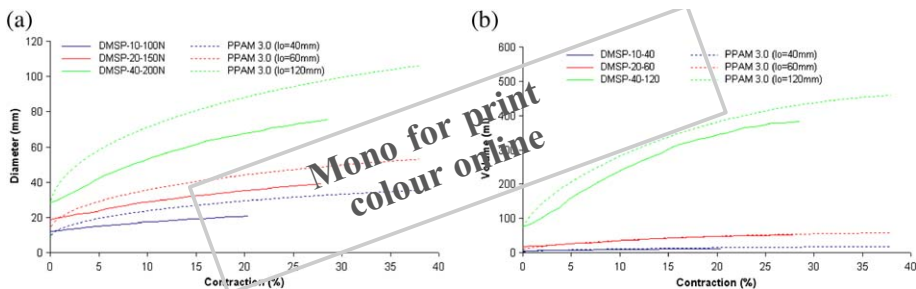


Figure 9. (a) Measured diameters for Festo fluidic muscles: DMSP-10-100N, DMSP-20-150N, and DMSP-40-200N and theoretical diameters for PPAM 3.0 as a function of contraction and (b) approximated volumes for Festo fluidic muscles: DMSP-10-40N, DMSP-20-60N, and DMSP-40-120N and theoretical volumes for PPAM 3.0 as a function of contraction.

DMSP-10-100, they both will present the same tension intensity curve. Following a similar reasoning, it is concluded that it is also constant for PPAM with a specific slenderness. According to Equations (1) and (4) both the maximum tension F_{\max} and the cross-section area $\left(\frac{\pi D^2}{4}\right)$ are proportional to l_0^2 and the PPAM's tension intensity can be expressed as:

$$\text{T.I.} = \frac{4}{\pi} \frac{f_{\max}\left(\frac{l_0}{R}\right)}{d_0^2\left(\epsilon, \frac{l_0}{R}\right)} \quad (7)$$

with $f_{\max}\left(\frac{l_0}{R}\right) = \frac{F_{\max}\left(l_0^2, \frac{l_0}{R}\right)}{l_0^2}$. Figure 10 presents a tension intensity comparison between Festo and PPAM actuators as a function of contraction. It is seen that Festo muscles present higher tension intensities than PPAMs with slenderness 9.6 reaching advantages of 200%. Since the actuator maximum cross-section area at low contractions is that of the end fittings, the tension intensity is constant until the membrane's equatorial diameter exceeds the diameter of the end fittings, which is not visible on the figure.

Using the maximum diameter at maximum contraction (which was expressed by the dimensionless maximum diameter $d_{0\max}$ of a PPAM defined by Daerden [17]) the influence of the slenderness on this ratio can be analyzed. As can be observed in Table 2, an increment in the muscle slenderness increases the actuator's tension intensity at maximum contraction.

4.5. Force-to-Mass Ratio

The force-to-mass ratio makes PAMs very attractive for a wide range of applications such as manipulators, mobile robots and rehabilitation devices. It is defined as the ratio of the actuator's maximum output force and the actuator's mass.

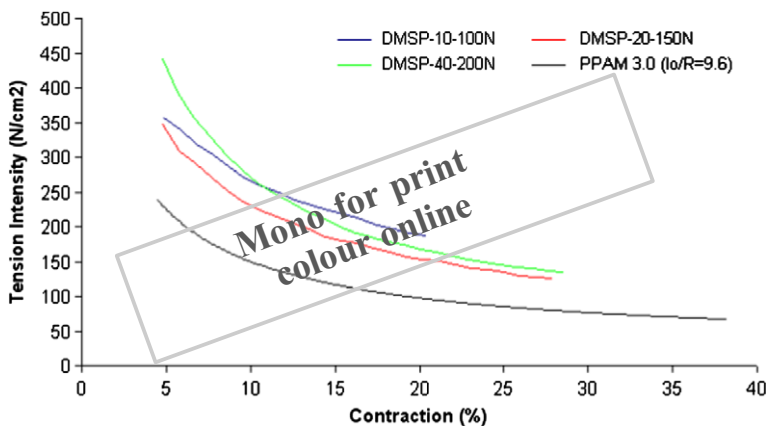


Figure 10. Tension intensity comparison between PPAM and Festo actuators as a function of contraction at 4 bar.

Table 2.

Influence of the slenderness on the tension intensity at maximum contraction of the PPAM

Slenderness	3	4	5	6	8	10	15	20
T.I.@max.contraction (N/cm ²)	32.1	39.8	45.8	50.6	57.7	62.7	70.5	74.9

The muscles mass is divided into the endings mass m_{end} and the membrane mass m_{mem} . In the case of McKibben-like muscles, the mass of the membrane is proportional to the muscle's length and defined by Festo as additional weight per 1 m length ($m_{\text{mem}} = XL$) with m expressed in g and L expressed in m. According to the technical data [16], the weight of each model with an axial (AM) and a radial (RM) pneumatic connection can be expressed as:

$$m_{\text{DMSP-10-AM-RM}} = 75 + 94L \quad (8)$$

$$m_{\text{DMSP-20-AM-RM}} = 202 + 178L \quad (9)$$

$$m_{\text{DMSP-40-AM-RM}} = 767 + 340L \quad (10)$$

In the case of the PPAM, the endings mass includes the end fittings m_{end1} and additional connectors m_{end2} . In order to parameterize the mass of a PPAM with a specific slenderness for any muscle size, the mass contributions of the different parts of the muscle are calculated. And, due to the specific geometry some of the mass coefficients can be scaled. Although the same additional connectors are used for any muscle size, the end fittings are scaled according to the membrane size and their mass can be expressed as:

$$m_{\text{end1}} = Al_0^2 \quad (11)$$

The PPAM's membrane is composed by the the pleated fabric and the high-tensile fibres. Although the fibres mass m_{mem1} is proportional to the actuator's length:

$$m_{\text{mem1}} = Bl_0 \quad (12)$$

the fabric mass m_{mem2} cannot be represented by a linear function. Since the cross section of the pleated fabric has to ensure that enough material will be available for the muscle to inflate to its full extent, its mass depends on the actuator's maximum length l_0 and diameter D (which is itself proportional to l_0 , see Equation (4)). And, therefore it is proportional to l_0^2 for a specific slenderness:

$$m_{\text{mem}2} = Cl_0^2 \quad (13)$$

To extend this parametrization of PPAMs with specific slenderness to series configurations of M modules, the ring mass m_{ring} is also included:

$$m_{\text{PPAM}} = m_{\text{end}1} + m_{\text{end}2} + M(m_{\text{mem}1} + m_{\text{mem}2}) + (M - 1)m_{\text{ring}} \quad (14)$$

5
AQ2  According to the mass measurements done on PPAM prototypes, the mass coefficients of PPAMs with slenderness values of 9.6 were calculated (Table 3).

10 Figure 11(a) shows how an increment in the PPAM size improves the force-to-mass ratio reaching values over 100 kN/kg for lengths up to 0.5 m. It is also seen how an increment on the number of modules (each point represents a series configuration with a different number of modules) reduces this ratio because of the inclusion of the rings. The reduction of the force-to-mass ratio over the total PPAM length is similar to that of Festo muscles, however, comparing muscles
15 with the same force ranges, PPAM has a better force-to-mass ratio than Festo muscles for any size. The difference becomes more important for larger muscle sizes reaching an improvement of 675% in the comparison between a 120 mm PPAM and DMSP-40.

4.6. Energy-to-Mass Ratio

20 The energy-to-mass ratio is defined by the actuator's maximum energy output and its mass. Although the load displacement is proportional to the muscle's length for both PAM types, the output force is length independent for Festo models and length squared dependent for PPAMs with constant slenderness (9.6). After calculating the maximum output energy from the measured data for
25 both muscles types with maximum working pressure of 4 bar, it is possible to extrapolate it to any muscle configuration.

$$E_{\text{PPAM}} = 76312.85l_0^3M \quad (15)$$

$$E_{\text{DMSP-10}} = 28.8368L \quad (16)$$

$$E_{\text{DMSP-20}} = 137.0475L \quad (17)$$

Table 3.

Mass coefficients of PPAMs with slenderness values of 9.6

A (g/m ²)	$m_{\text{end}2}$ (g)	B (g/m)	C (g/m ²)	m_{ring} (g)
32.1	60	39.8	45.8	2

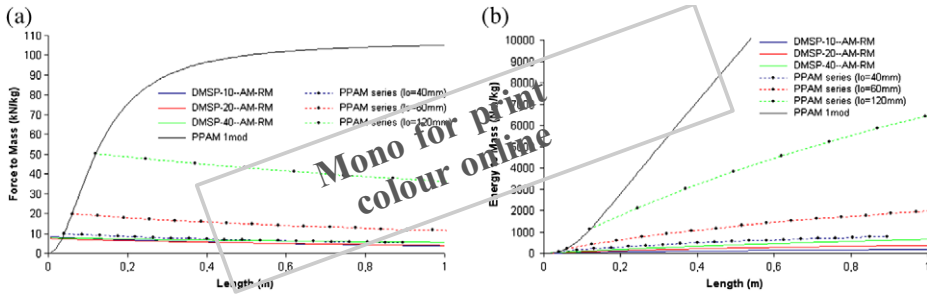


Figure 11. (a) Force-to-mass ratio comparison between PPAM and Festo actuators and (b) energy-to-mass ratio comparison between PPAM and Festo actuators at 4 bar.

$$E_{DMSP-40} = 727.4334L \tag{18}$$

Figure 11(b) shows how an increment in the PPAM size improves the energy-to-mass ratio reaching values over 10,000 Nm/kg for lengths up to 0.5 m. It is also seen how an increment of the number of modules increases this ratio. This is because the output energy is proportional to the number of modules but the rings are much more lightweight than the end fittings. Comparing muscles with the same force ranges, PPAM has a better ratio than Festo muscles for any size. The difference become more important with the muscle size reaching improvements over 1000% in the comparison between a 120 mm PPAM and DMSP-40.

4.7. Energy-to-Volume Ratio

As was explained in previous sections, a McKibben-like muscle keeps a cylindrical shape during the inflation and both output energy and volume are proportional to the muscle's maximum length (see Sections 4.3 and 4.6). Therefore, the energy-to-volume ratio is a constant for each Festo model. In the case of PPAMs, as their output energy and volume depend on the muscle length cubed, see Equations (5) and (15), the energy-to-volume ratio of a PPAM with a specific slenderness is constant on any muscle size. Furthermore, as the rings positioned between the modules in a PPAM series configuration do not contract, the output energy is proportional to the number of modules, but the volume is slightly

Energy to Volume ratio (Nm/l)			
Festo	DMSP-10-...	DMSP-20-...	DMSP-40-...
	268,50	159,08	227,84
PPAM	lo=40mm	lo=60mm	lo=120mm
1 module	287,11	287,11	287,11
Serie configuration (L _{TOTAL} =1m)	282,76	284,23	285,74

Figure 12. Energy to volume ratio comparison between PPAM and Festo actuators at 4 bar.

Properties	Units	Festo Fluidic Muscle			PPAM (l ₀ /R=9,56)		
		DMSP-10	DMSP-20	DMSP-40	l ₀ =40mm	l ₀ =60mm	l ₀ =120mm
Max Tension	N	630	1500	6000	660	1487	5950
Max Diameter	mm	20.7	39	75.4	35.4	53	106.1
Max contraction (4 bar)	%	13	22.8	28.3	1 mod - 38.2 5 mod - 34.7 10 mod - 34.3 20 mod - 34.1	1 mod - 38.2 4 mod - 36.0 8 mod - 35.6 15 mod - 35.4	1 mod - 38.2 2 mod - 37.4 3 mod - 37.0 4 mod - 36.8
Tension intensity @ max contraction	kN/m ²	1516.3	1255.6	1473.6	618.2	618.2	618.2
Force to Mass	kN/kg	l ₀ =40mm - 8	l ₀ =60mm - 7.1	l ₀ =120mm - 7.4	1 mod - 9.8	1 mod - 19.7	1 mod - 50.2
Energy to Mass	Nm/kg	l ₀ =40mm - 14.6	l ₀ =60mm - 38.7	l ₀ =120mm - 108.1	1 mod - 72.7	1 mod - 218.5	1 mod - 1112
Energy to Volume	Nm/l	268.5	159.1	227.8	1 mod - 287.1	1 mod - 287.1	1 mod - 287.1

Figure 13. Concluding table of the comparison between PPAM and Festo actuators.

larger than the sum of those of the modules, see Equation (6). Therefore, the PPAM energy-to-volume ratio is slightly diminished because the use of a series arrangement with a maximum difference of 1.5%. In any case, PPAM has a better ratio than Festo muscles of any size reaching improvements over 180% in the comparison with DMSP-20 (see Fig. 12).

4.8. Concluding Table

In Fig. 13 a concluding comparison is made for both muscle types.

5. Conclusion

This paper describes the third-generation PPAM and presents a comparison with a McKibben like commercially available muscle, the Festo fluidic muscle.

The third generation PPAM is more compact and the use of 3D printing technology causes a 55% reduction of the weight of the muscle. The production process is drastically simplified because of the use of a continuous high-tensile fibre and toothed-end fittings, which serve to give the correct folded shape to the membrane and to align the fibres. The new production process is very flexible: PPAMs can now be produced in all sizes from 4 to 50 cm and the building time has been reduced by 75%.

It has been shown that the PPAM can be dimensioned to have similar force ranges as commercially available Festo muscles. Although Festo muscles are thinner than PPAMs, PPAM 3.0 is much more lightweight, and therefore it presents better force-to-mass and energy to mass ratios than Festo models. Due to the similarities with the commercially available muscles and mentioned advantages, PPAMs are very suitable for a wide range of robotic and automation applications.

We have analyzed the static characteristics of the third generation PPAM. Of course, the influence of the muscle dimensions needs to be investigated according to the production limitations. Therefore, several PPAM configurations need to be tested in order to analyze the hysteresis and radial stress, which are not currently included in the mathematical model.

Acknowledgment

This work has been funded by the European Commission's 7th Framework Program as part of the project VIACTORS under Grant no. 231554.

References

1. B. Vanderborght, R. Van Ham, B. Verrelst, M. Van Damme and D. Lefeber, Overview of the Lucy project: dynamic stabilization of a biped powered by pneumatic artificial muscles, *Adv. Robotics* **22**(25), 1027–1051 (2008). 5
2. K. Hosoda, T. Takuma, A. Nakamoto and S. Hayashi, Biped robot design powered by antagonistic pneumatic actuators for multi-modal locomotion, *Robotics Auton. Syst.* **56**(1), 46–53 (2008).
3. M. Van Damme, B. Vanderborght, B. Verrelst, R. Van Ham, F. Daerden and D. Lefeber, Proxy-based sliding mode control of a planar pneumatic manipulator, *Int. J. Robotics Res.* **28**(2), 266–284 (2009). 10
- AQ4 4. H. Gattringer, R. Naderer and H. Bremer, Modeling and control of a pneumatically driven Stewart platform. *Motion Vibration Control*, pp. 93–102 (2009). 15
5. P. Beyl, M. Van Damme, R. Van Ham, B. Vanderborght and D. Lefeber, Design and control of a lower limb exoskeleton for robot-assisted gait training, *Appl. Bionics Biomech.* **6**(2), 229–243 (2009).
6. R. Versluys, B. Vanderborght, D. Lefeber and J. Naudet, IPPAM: intelligent prosthesis actuated by pleated pneumatic artificial muscles: objectives and mechanical concept, in *Int. Conf. on Climbing and Walking Robots (CLAWAR 2006)*, Brussels, pp. 475–484 (2006). 20
7. Daniel P. Ferris, Joseph M. Czerniecki and Blake Hannaford, An ankle-foot orthosis powered by artificial pneumatic muscles', *J. Appl. Biomech.* **21**(2), 189–197 (2005).
8. D. G. Caldwell and N. Tsagarakis, Biomimetic actuators in prosthetic and rehabilitation applications, *Technol. Health Care* **10**, 107–120 (2002).
9. C. Chou and B. Hannaford, Measurement and modelling of Mckibben pneumatic artificial muscles, *IEEE Trans. Robotics Automat.* **12**(February), 90–102 (1996). 25
- AQ5 10. G. Ingeg, 'Romac actuators for micro robots', in: *Proc. IEEE Micro Robotics and Teleoperators Workshop*, Hyannis, MA (1987).
11. H. A. Baldwin, Realizable models of muscle function, in *Proc. First Rock Biomechanics Symposium*, New York, NY, pp. 139–148 (1969). 30
12. H. F. Schulte, The characteristics of the Mckibben artificial muscle, *Appl. External Power Prosthet. Orthot.* **874**, 94–115 (1961).
13. K. Inoue, Rubberactuators and applications for robotics, in: *Proc. 4th Int. Symp. on Robotics Research*, Tokyo, pp. 57–63 (1987).
14. Shadow Robot Company, Design of a dextrous hand for advanced CLAWAR applications, in: *Proc. 6th Int. Conf. on Climbing and Walking Robots and the Support Technologies for Mobile Machines*, Catania, Italy, pp. 691–698 (2003). 35
15. Merlin Systems Corporation, Merlin actuators: automation, animatronics and artificial creatures, Brochure Merlin Actuators (2003).
16. Festo, Fluidic muscle mas, *Festo Brochure Fluidic Muscle* (2004). 40
17. F. Daerden, Conception and realization of pleated pneumatic artificial muscles and their use as compliant actuation elements, PhD thesis, Vrije Universiteit Brussel (1999).

22

D. Villegas et al. / Advanced Robotics XX (2012) XXX–XXX

18. B. Verrelst, R. Van Ham, B. Vanderborght, F. Daerden and D. Lefeber, The pneumatic biped LUCY actuated with pleated pneumatic artificial muscles, *Auton. Robot* **18**, 201–213 (2005).
19. R. Versluys, A. Desomer, G. Lenaerts, O. Pareit, B. Vanderborght, G. Perre, L. Peeraer and D. Lefeber, A biomechatronical transtibial prosthesis powered by pleated pneumatic artificial muscles, *Int. J. Model. Ident. Control* **4**(4), 394–405 (2008).
20. B. Verrelst, R. Van Ham, B. Vanderborght, D. Lefeber, F. Daerden and M. Van Damme, Second generation pleated pneumatic artificial muscle and its robotic applications, *Adv. Robotics* **20**(7), 783–805 (2006).
21. Y. K. Lee and I. Shimoyama, A skeletal framework artificial hand actuated by pneumatic artificial muscles, *Morpho-functional machines: the new species: designing embodied intelligence*, pp. 131–143 (2003).
22. B. Tondu and P. Lopez, Modeling and control of McKibben artificial muscle robot actuators, *IEEE Control Syst. Mag.* **20**(2), 15–38 (2000).
23. M. Van Damme, P. Beyl, B. Vanderborght, R. Van Ham, V. Innes and L. Dirk, Modeling hysteresis in pleated pneumatic artificial muscles, in: *IEEE Int. Conf. on Robotics, Automation & Mechatronics (RAM)*, Chengdu, China, pp. 471–476 (2008).

About the Authors



Daniel Villegas was born in Pamplona, Spain, in 1985. He received his master in electronic engineering from Universidad Pública de Navarra (UPNA) in 2009. His research focused on the production, characterization and measurement of the third generation Pleated Pneumatic Artificial Muscle. He is currently working in the “Recycling and reusing WEEE (Waste Electrical and Electronic Equipment) department” of the “Fundación Traperos de Emaús Navarra” in Navarra, Spain.



Michaël Van Damme received his master’s degree in electrical engineering at the Vrije Universiteit Brussel in 2001. He has been a full-time researcher at the Vrije Universiteit Brussel since 2003, and received the PhD degree in engineering from the Vrije Universiteit Brussel in 2009. He is currently a postdoctoral researcher interested in compliant actuation, robot safety, physical human-robot interaction and rehabilitation robotics.



Bram Vanderborght received his degree in mechanical engineering at the Vrije Universiteit Brussel (VUB) in 2003 and PhD degree in applied sciences in May 2007. The focus of his research was the use of adaptable compliance of pneumatic artificial muscles in the biped Lucy. In May–June 2006 he was guest researcher in AIST-JRL Lab in Tsukuba and from October 2007 to April 2010, he worked as postdoctoral researcher at the Italian Institute of Technology (IIT). Since October 2009 he is professor at the VUB. His research interests include bipedal locomotion, compliant actuation, rehabilitation robotics, and safe and cognitive HRI.



Pieter Beyl joined the Robotics and Multibody Mechanics Research Group after receiving the master of science degree in mechanical engineering from Vrije Universiteit Brussel in 2005. He received the PhD degree in engineering from the Vrije Universiteit Brussel in 2010. His research interests include robot-assisted rehabilitation, human-robot interaction, powered exoskeletons and novel actuators.

5

10



Dirk Lefeber received his degree in civil engineering and PhD degree in applied sciences at the Vrije Universiteit Brussel in 1979 and 1986, respectively. He is currently a full professor and head of the Mechanical Engineering Department and the Robotics and Multibody Mechanics Research Group, Vrije Universiteit Brussel. His research interests include new actuators with adaptable compliance, dynamically balanced robots, robot assistants, rehabilitation robotics, and multibody dynamics.

15